The influence of membrane ion-permselectivity on electrokinetic concentration enrichment in membrane-based preconcentration units†

Dzmitry Hlushkou,[a] Rahul Dhopeshwarkar,[b] Richard M. Crooks*[c] and Ulrich Tallarek*[d]

Received 11th January 2008, Accepted 11th April 2008
First published as an Advance Article on the web 12th May 2008
DOI: 10.1039/b800549d

The performance of nanoporous hydrogel microplugs with varying surface charge density is described in concentrating charged analytes electrokinetically in a microfluidic device. A neutral hydrogel plug with a mean pore size smaller than the size of charged analytes acts as a simple size-exclusion membrane. The presence of fixed charges on the backbone of a nanoporous hydrogel creates ion-permselectivity which results in charge-selective transport through the hydrogel. This leads to the development of concentration polarization (CP) in the adjoining bulk electrolyte solutions under the influence of an applied electrical field. CP strongly affects the distribution of the local electrical field strength, in particular, in the vicinity of the hydrogel plug which can significantly reduce the concentration enrichment factors compared to the neutral hydrogel. A theoretical model and simulations are presented, together with experimental data, to explain the interplay of hydrogel or membrane cation-selectivity, electrical field-induced CP, and the distribution of the local electrical field strength with respect to concentration enrichment of negatively charged analytes at the cathodic membrane–solution interface.

Introduction

The control of mass and charge transport by means of membrane functionality integrated into multifunctional miniaturized devices demonstrates potential in a variety of disciplines.[1,2] Many applications are found in analytical chemistry, *e.g.*, for sample preparation, gating, sensing, and separation. On-chip preconcentration often is a crucial step in such applications. Therefore, a number of strategies have been developed during the last several years for improving detection limits in microfluidic-based assays using on-chip analyte concentration enrichment.[3–26] Some of these methods employ nanoporous structures, such as track-etched or laser-patterned membranes incorporated in microscale analysis systems, to achieve analyte enrichment *via* size-based filtration. An uncharged membrane acts as a simple physical barrier to electrophoretic transport of charged analytes which are size-excluded from the membrane pores, resulting in concentration enrichment at the membrane–bulk solution interface (see part (a) of Scheme 1). This basic principle was the motivation for concentrating charged analytes at size-exclusion membranes after the application of a voltage across the membrane.[6,19,21–23,25,26]

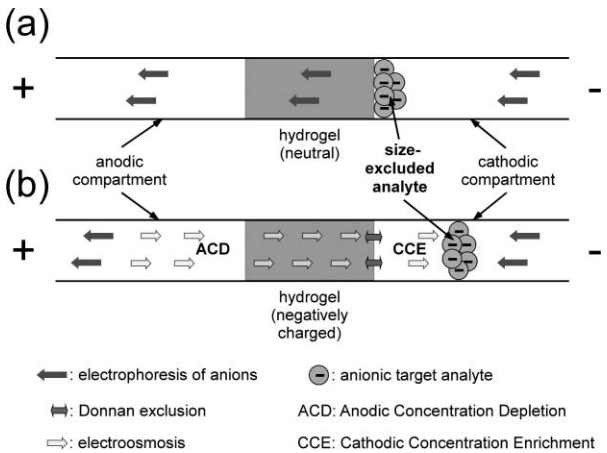

Scheme 1 Electrokinetic concentration enrichment of negatively charged analyte at/close to the cathodic bulk solution interface of a neutral (a) and an anionic (b) hydrogel plug or membrane.

For example, Khandurina *et al.*[6] and Foote *et al.*[21] achieved approximately 100- and 600-fold signal increases for DNA fragments and proteins, respectively, with functional units made of two separated microchannels and a silicate nanoporous bonding layer between the glass substrate and cover plate. Song *et al.*[19] observed a similar order of protein concentration in fused-silica microchips with two microchannels separated by a zwitterionic polymer membrane. In the work of Hatch *et al.*[25] two polymeric elements, a thin (~50 μm) size-exclusion membrane and a longer (~ cm) porous monolith, were fabricated *in situ* and integrated seamlessly for realizing on-chip preconcentration of proteins prior to protein sizing by sodium dodecyl sulfate–polyacrylamide gel electrophoresis. Successful integration of preconcentration with protein sizing was shown

[a]*Institut für Verfahrenstechnik, Otto-von-Guericke-Universität Magdeburg, Universitätsplatz 2, 39106, Magdeburg, Germany*
[b]*Department of Chemical Engineering, Texas A & M University, 3122 TAMU, College Station, TX, 77843-3122, USA*
[c]*Department of Chemistry and Biochemistry, The University of Texas at Austin, 1 University Station, A5300, Austin, TX, 78712-0165, USA. E-mail: crooks@cm.utexas.edu*
[d]*Department of Chemistry, Philipps-Universität Marburg, Hans-Meerwein-Strasse, 35032, Marburg, Germany. E-mail: tallarek@staff.uni-marburg.de*
† The HTML version of this article has been enhanced with colour images.

by rapid, more than 10^3-fold preconcentration and subsequent separations that exhibited the expected log-linear dependence of mobility on molecular weight. While the sieving polymer was tailored for size-based separations of proteins in the molecular mass range of *ca.* 20–200 kDa, the nanopores within the preconcentration membrane are small enough to exclude a wide range of proteins (>10 kDa), but are permeable for buffer ions.[25] While these examples demonstrate the great potential of size-exclusion membranes for electrokinetic preconcentration, the backbone of the membrane in most cases is at least slightly charged. This characteristic makes the nanoporous gel or membrane ion-permselective which, upon application of the electrical field, stimulates complex phenomena related to coupled mass and charge transport normal to the charge-selective interfaces. This behavior adds further contributions to the simple picture of size-based filtration which can adversely affect sample preconcentration efficiency and which, therefore, should be analyzed carefully in order to control and scale system performance.

If the walls of the membrane nanopores bare fixed charges, these matrices can be used for tailoring trans-membrane mass and charge transport through their ion-permselectivity.[27] The presence of fixed charges on the internal and external surface of the membrane gives rise to a Donnan electrical potential at the macroscopic membrane boundaries,[26–29] which reflects counterion enrichment and co-ion exclusion by the charged membrane at electrochemical equilibrium. For instance, an anionic hydrogel plug acts as a cation-selective membrane for the permeating ions of the background buffer (see part (b) of Scheme 1). In general, the control of pore size, pH and ionic strength of the external mobile phase, as well as surface charge allows one to direct trans-membrane mass and charge transport through a multiple-barrier approach.[30–36]

As an electrical field is applied to a cation-selective membrane, the flow of electrical current is accomplished nearly exclusively by the counterions (cations). The transport number of the counterion (or the sum of the transport numbers of all counterionic species) is nearly unity, *i.e.*, the fractional electrical current carried by the counterions within the membrane phase is much larger than the corresponding value within the bulk liquid phases. As a consequence, ion concentration gradients result at the membrane–solution interfaces: enriched and depleted concentration polarization (CP) zones form in the bulk, quiescent solutions adjacent to the cathodic and anodic interfaces of the cation-selective membrane, respectively.[26,27] The efficiency of concentration enrichment with a charged membrane is therefore strongly influenced by the actual intensity of CP. It has been reported that CP is responsible for sample destacking, nonlinear concentration enrichment factors, and a lack of reproducibility.[21,25,26] The analysis of the effect of membrane ion-permselectivity on the dynamics and efficiency of electrokinetic concentration enrichment is still limited.[26,37] On the other hand, if this knowledge were available the important step of sample concentration prior to analysis can become a powerful and also reliable tool in the development of multifunctional lab-on-a-chip devices.

The study presented here compares the physicochemical behavior of neutral and anionic hydrogel microplugs (uncharged *vs.* charged membranes) in determining the efficiency of electrokinetic concentration enrichment inside the adjoining microfluidic channels. Under the influence of an applied electrical field, a neutral hydrogel (uncharged membrane) can only act as a physical barrier to the electrophoretic flux of a negatively charged analyte, resulting in concentration enrichment at the interface between the hydrogel microplug and the buffer solution within the channel. However, when a negatively charged hydrogel is used, the behavior of the system becomes far more complex. The development of CP redistributes the local electrical field within the microchannel which, in turn, governs the efficiency of analyte concentration enrichment. We employ a simple theoretical model and simulations to analyze the observed dynamics of electrokinetic filtering by nanoporous hydrogel microplugs integrated into straight microfluidic channels.

Experimental section

Chemicals

The silicone elastomer and curing agent (Sylgard 184) used to prepare the poly(dimethylsiloxane) (PDMS) microfluidic devices were obtained from K. R. Anderson, Inc. (Morgan Hill, CA). Bovine serum albumin (BSA) conjugated with Alexa Fluor 488 was obtained from Molecular Probes (Eugene, OR). Acrylic acid (AA), 2-hydroxyethyl methacrylate (HEMA), ethylene glycol dimethacrylate, and Irgacure 651 (Sigma-Aldrich, St. Louis, MO) were used for preparing the photopolymerizable hydrogel precursors. Molecular biology grade 1 M TRIS-HCl buffer (Fisher Biotech, Fair Lawn, NJ) was diluted to 10.0 mM (pH 8.1) with deionized water (18 MΩ cm, Milli-Q® Gradient System, Millipore) and used as background electrolyte in all experiments.

Microfluidic device fabrication

The PDMS/glass hybrid microfluidic devices employed for the concentration enrichment experiments were fabricated by the replica molding technique.[38] First, holes (~2.5 mm in diameter) were punched in a PDMS monolith (~5 mm thick) to serve as reservoirs for fluidic delivery. The monolith was then bonded irreversibly to a pre-cleaned cover glass (25 mm × 25 mm, 0.13–0.17 mm thick, VWR Scientific) after both were treated with an O_2 plasma (60 W, model PDC-32G, Harrick Scientific, Ossining, NY) for 15 s. The bonding process was allowed to proceed for at least 2 min before introducing liquids into the microchannel. The ensuing microfluidic design (Fig. 1a) included a straight microchannel (approximately 100 μm wide × 20 μm deep × 6 mm long) connecting the two 2.5 mm-diameter reservoirs (ResA and ResB). This microchannel design does not incorporate side channels, which were used in some of our previous studies to remove unwanted hydrogel precursor from the channel following photopolymerization.[22]

Hydrogel microplug fabrication

The hydrogel microplug was fabricated within the microchannel using a previously reported photopolymerization procedure.[22,37] First, the precursor solution was allowed into the microchannel by capillary action. Next, UV light (365 nm, 200 s, 300 mW cm^{-2},

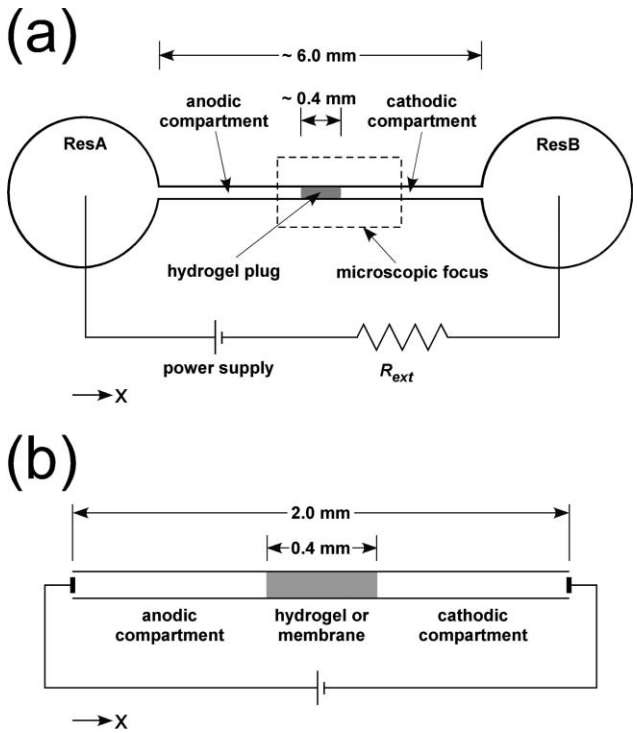

Fig. 1 (a) Schematic illustration of the experimental device used for electrokinetic concentration enrichment. (b) Schematic illustration of the system used for the simulation of analyte concentration enrichment in a microfluidic channel containing a fixed nanoporous (anionic or neutral) membrane.

EFOS Lite E3000, Ontario, Canada) was projected onto the central part (~400 μm long) of the channel from the side port of a microscope (DIAPHOT 300, Nikon) through a 10× objective lens. The UV exposure resulted in polymerization of the precursors in the illuminated region. To remove the unpolymerized precursor solution, 10.0 mM TRIS-HCl buffer was loaded into the reservoirs (ResA and ResB) and allowed to fill the microchannel for about 90 min. A bias was then applied between coil electrodes (90% Pt/10% Ir, 0.25 mm in diameter and 50.0 mm in length) placed at the centers of the 2.5 mm-diameter reservoirs. Thus, the distance between the two 0.25 mm-diameter electrodes in the experimental device is *ca.* 8.25 mm, and an applied bias of, *e.g.*, 100 V translates to an electrical field strength of about 12 kV m^{-1}. The necessary electrical bias was achieved using a custom-built power supply constructed using a high-voltage (range 0–1067 V) output module from Ultra Volt (Ronkonkoma, NY). Custom software allowed the voltages to be changed with 100 ms time resolution. For the anionic hydrogels (AA copolymerized with HEMA), the unwanted precursor (bearing negative charges) was removed electrophoretically using low biases of 50–150 V. The neutral hydrogel remnants cannot be removed electrophoretically, but it was possible to remove these residues *via* electroosmotic flow induced within the channel by applying biases of up to 400 V.

Data acquisition and analysis

Prior to each experiment, ResA and ResB were rinsed with 10.0 mM TRIS-HCl buffer, and then 25 μL of 500.0 nM BSA–Alexa Fluor conjugate in 10.0 mM TRIS-HCl buffer was loaded into each reservoir. Finally, a bias voltage was applied between the electrodes in the two reservoirs, and simultaneously fluorescence micrographs were captured (V++ microscopy imaging, Digital Optics, New Zealand) over the microchannel region incorporating the hydrogel using an inverted epifluorescence microscope (Eclipse TE 2000-U, Nikon, Japan) equipped with a CCD camera (Cascade 512B, Photometrics, Tuscon, AZ). A typical sequence of micrographs included 541 frames (4× objective lens, 1 × 1 binning, 512 × 290 pixels) at a rate 2 s $frame^{-1}$ (exposure time 100 ms) captured over 1080 s. For superior visual quality, the images were edited to an appropriate grayscale and a false color scheme was added (brightness decreasing in the order white–green–blue–black).

Fluorescence intensity data were determined from the captured sequence of micrographs and then quantified in terms of analyte enrichment factors. This was accomplished as follows. A section of the channel under the microscopic focus (see Fig. 1a) was chosen as a region of interest. Fluorescence intensities were averaged over the microchannel cross-section and profiled along the channel (*x*-axis) at different time intervals. The corresponding enrichment factors were calculated by dividing the peak heights in the fluorescence intensity profiles by the average fluorescence intensity obtained in a separate reference channel containing the fluorescent analyte. Fluorescence intensity values were corrected by subtracting the background count and normalized with respect to the maximum intensity reading for plotting fluorescence intensity profiles.

Numerical simulations

The hydrogel plug fixed in the microfluidic device connects two microchannel compartments, the anodic compartment (positive electrode) and the cathodic compartment (grounded electrode), *via* nanometer-sized pores. The microfluidic-nanofluidic phase boundaries in the analyzed system are referred to as the anodic and cathodic hydrogel plug-microchannel solution interfaces. The hydrogel reduces the cross-sectional area available for the passage of ionic current which increases the electrical resistance of the microchannel.[37] The small pores of the hydrogel, having a diameter of only a very few nanometers, provide strong resistance to hydraulic flow and cause significant pore-level electrical double layer overlap. Thus, (electro)hydrodynamic flow is here neglected and the focus is solely on the varying surface charge density (and the resulting ion-permselectivity) of a hydrogel plug in view of electrical field-induced CP and its influence on the concentration enrichment efficiency for negatively charged analyte at/close to the cathodic hydrogel plug-microchannel solution interface. In general, there exists a finite (albeit small) cathodic electroosmotic flow component inside the anionic hydrogel and adjoining microchannels.[22] We have analyzed its effect on the intensity and location of the enriched tracer zone in the cathodic microchannel compartment in a previous article.[37] It was shown that the interplay of membrane ion-permselectivity, tracer electrophoresis, and bulk electroosmotic flow contributed to a coupled transport scheme and complex transient behavior in the system which eventually prevented the tracer zone from finding a stable position in the cathodic microchannel. Therefore, we decided to complement this earlier work[37] and focus in the simulations of this work solely

on the effect of membrane ion-permselectivity on electrical field distribution and electrokinetic concentration enrichment with the experimental microfluidic device illustrated in Fig. 1a.

In this study we employed an approach based on the numerical solution of the coupled Nernst–Planck and Poisson equations as well as the continuity equations in order to simulate electrokinetic transport in the microfluidic system illustrated by Fig. 1a. The geometry of the simulated device shown in Fig. 1b is reduced to a straight microchannel (L = 2 mm) fitted with a flat, porous membrane (L = 400 μm) at its center; that is, the membrane covers the distance from x = 800 μm to x = 1200 μm. It is assumed that the microchannel is terminated by two relatively large reservoirs containing the electrodes. Thus, the distance between the electrodes in the simulations is 2 mm (Fig. 1b), in contrast to the experimental device where this distance is *ca.* 8.25 mm (Fig. 1a). The membrane is treated as a pseudo-homogeneous material, *i.e.*, as homogeneous domain characterized by effective morphological, material, and transport characteristics (dielectric constant, volume density of the fixed electrical charge, apparent diffusion coefficient, *etc.*). In addition, it is assumed that the system is isothermal, in particular, there are no Joule heating effects, and that there is no chemical reaction in the system (including water dissociation) and adsorption–desorption taking place at the solid–liquid (wall and membrane) interfaces. Finally, it is assumed that no wall-effects exist and, therefore, the geometry can be reduced to a one-dimensional configuration where parameters vary only along the x-axis (Fig. 1b).

The general transport of ions of the buffer solution and of the analyte molecules due to an applied bias is governed by a conservation law

$$\frac{\partial c_i(x,t)}{\partial t} = \frac{\partial}{\partial x}\left(D_i(x)\frac{\partial c_i(x,t)}{\partial x} + z_i c_i(x,t) D_i(x)\frac{F}{RT}\frac{\partial \phi(x,t)}{\partial x} \right), \quad (1)$$

where c_i is the molar concentration of ionic species i, D_i and z_i are its diffusion coefficient and valency, respectively, ϕ is the local electrical potential, and F, R and T represent the Faraday constant, molar gas constant and temperature, respectively. The local concentration of the ions and the local electrical potential are related by the Poisson equation

$$\frac{\partial^2 \phi(x,t)}{\partial x^2} = -\frac{\rho_{\text{fix}}}{\varepsilon_0 \varepsilon_r} - \frac{\rho_e(x,t)}{\varepsilon_0 \varepsilon_r} = -\frac{\rho_{\text{fix}}}{\varepsilon_0 \varepsilon_r} - \frac{F}{\varepsilon_0 \varepsilon_r}\sum_i z_i c_i(x,t), \quad (2)$$

where ρ_e is the volume charge density of the electrolyte solution, ρ_{fix} is the volume fixed-charge density of the membrane associated with the surface charge on the pore walls, and ε_0 and ε_r are the vacuum permittivity and dielectric constant, respectively. The value of ρ_{fix} is determined by the surface charge density on the membrane pore walls and by the volume-to-surface ratio for the membrane. Thus, the spatiotemporal behavior of the ionic concentrations can be obtained by solution of the coupled partial differential eqns (1) and (2) subjected to the corresponding boundary and initial conditions.

In this study, the following boundary and initial conditions were used (indices 1 and 2 correspond to the cations and anions of the background buffer, while index 3 corresponds to the charged tracer molecules)

$$c_1(x=0,\,t) = c_1(x=L,\,t) = c_{1,\text{res}},\; c_2(x=0,\,t) = c_2(x=L,\,t) = c_{2,\text{res}},\; c_3(x=0,\,t) = 0,\; c_3(x=L,\,t<t_{\text{start}}) = 0,\; c_3(x=L,\,t_{\text{start}} < t < t_{\text{fin}}) = c_{3,\text{res}},\; c_3(x=L,\,t>t_{\text{fin}}) = 0,\text{ and } \phi(x=0,\,t) = V,$$
$$\phi(x=L,\,t) = 0,$$

where $c_{1,\text{res}}$ and $c_{2,\text{res}}$ are the constant concentrations of the buffer ions in the reservoirs and V is the applied bias. Twice negatively charged tracer (analyte) molecules are introduced into the channel from the right (cathodic) reservoir as a pulse/slug with a constant concentration $c_{3,\text{res}}$ = 5 μM. The product of the pulse duration t_{fin}–t_{start} and $c_{3,\text{res}}$ defines the total amount of injected tracer molecules, N_{trac}. In this study, $t_{\text{start}} = 0$ and $N_{\text{trac}} = 6.022 \times 10^7$, while t_{fin} is determined by the magnitude of the applied voltage. The constant N_{trac} facilitates the comparison of simulated enrichment factors for different voltages. The enrichment factor for the tracer zone is determined as the ratio $c_{3,\text{EZ}}/c_{3,\text{res}}$, where $c_{3,\text{EZ}}$ is the highest concentration in the steady-state tracer profile (enrichment zone) in the cathodic compartment of the microchannel.

The other physical parameters used in the simulations are given in Table 1. For example, the diffusion coefficient of the background ions inside the membrane is reduced due to tortuosity of the nanopore space compared with the straight microchannel compartments. A reduction by a factor of two is here assumed due to the geometry and topology of the interconnected nanopores. Further, because tracer molecules are usually larger than the background ions their diffusion coefficient in bulk solution has been reduced (by a factor of slightly more than three) compared to the background ions. With this diffusion coefficient the resulting electrophoretic mobility of the twice negatively charged tracer molecules employed in the simulations becomes comparable to that of the BSA molecules used in the experiments. In addition, the zero for the diffusion coefficient of tracer molecules inside the membrane simulates their complete size-exclusion from the membrane nanopores at the macroscopic level.

Table 1 Physical parameters employed for the simulations

Parameter	Anodic compartment	Membrane	Cathodic compartment
Diffusion coefficient of positive electrolyte ion/m^2 s^{-1}	1.5×10^{-9}	0.75×10^{-9}	1.5×10^{-9}
Diffusion coefficient of negative electrolyte ion/m^2 s^{-1}	1.5×10^{-9}	0.75×10^{-9}	1.5×10^{-9}
Diffusion coefficient of tracer species/m^2 s^{-1}	0.45×10^{-9}	0	0.45×10^{-9}
Dielectric constant	80	80	80
Ionic concentration of electrolyte in reservoirs/mM	5	—	5
Tracer concentration in reservoirs/mM	0	—	0.005
Volume fixed-charge density of membrane/mM	—	0, 0.5, and 5	—

Coupled eqns (1) and (2) were resolved by a parallel code based on lattice algorithms. For the solution of the Poisson and Nernst–Planck equations, respectively, the numerical approaches proposed by Warren[39] and by Capuani *et al.*[40] were employed. Although the investigated system was reduced to a one-dimensional one, both numerical schemes were implemented in three dimensions. This provides a means to apply the numerical model to studies of more complex two- and three-dimensional systems. In the present study, a uniform computational grid ($1000 \times 3 \times 3$)Δh was used with a space step of $\Delta h = 2\,\mu$m. The system was assumed to be homogeneous along transverse dimensions. The temporal behaviour was obtained with a time step of $\Delta t = 5 \times 10^{-5}$ s. At each time step, the Poisson equation was solved 10 times with an under-relaxation factor of 0.25 in order to ensure numerical stability. Then, updated values of the local electrical potential were used to resolve the Nernst–Planck equation. A single numerical simulation (for a selected value of the electrical field strength and fixed-charge density of the membrane) required about 48 h at 20 processors of a HP Superdome supercomputer in order to analyze the temporal behavior of the system for 500 s.

Results and discussion

Neutral hydrogel microplug as a physical barrier

The fluorescence micrographs shown in Fig. 2a and 2b demonstrate the role of a neutral hydrogel microplug for impeding the electrophoretic migration of negatively charged BSA. Fig. 2a is a micrograph obtained before application of an electrical field, and Fig. 2b was obtained after applying a forward bias (ResA at positive potential and ResB grounded) of 100 V for 960 s. The applied voltage induces migration of BSA in ResB towards the plug. However, the nanoporous hydrogel imposes a physical limitation on the further migration of BSA towards ResA. It is a consequence of the size of BSA (MW ~ 66 kDa, size 4.0 × 14.0 nm)[41] compared to the diameter of the pores (~2 nm)[22,42] in the hydrogel matrix. Accordingly, BSA is concentrated at the cathodic hydrogel plug–microchannel solution interface. Thus, concentration enrichment of proteins is easily achieved by moving them continuously against the "fine mesh" of a membrane whose pores are small enough for such large analytes, but permeable for buffer ions. Whether or not a protein is held at the membrane depends on the field strength, diffusivity of the protein, and the partition coefficient.

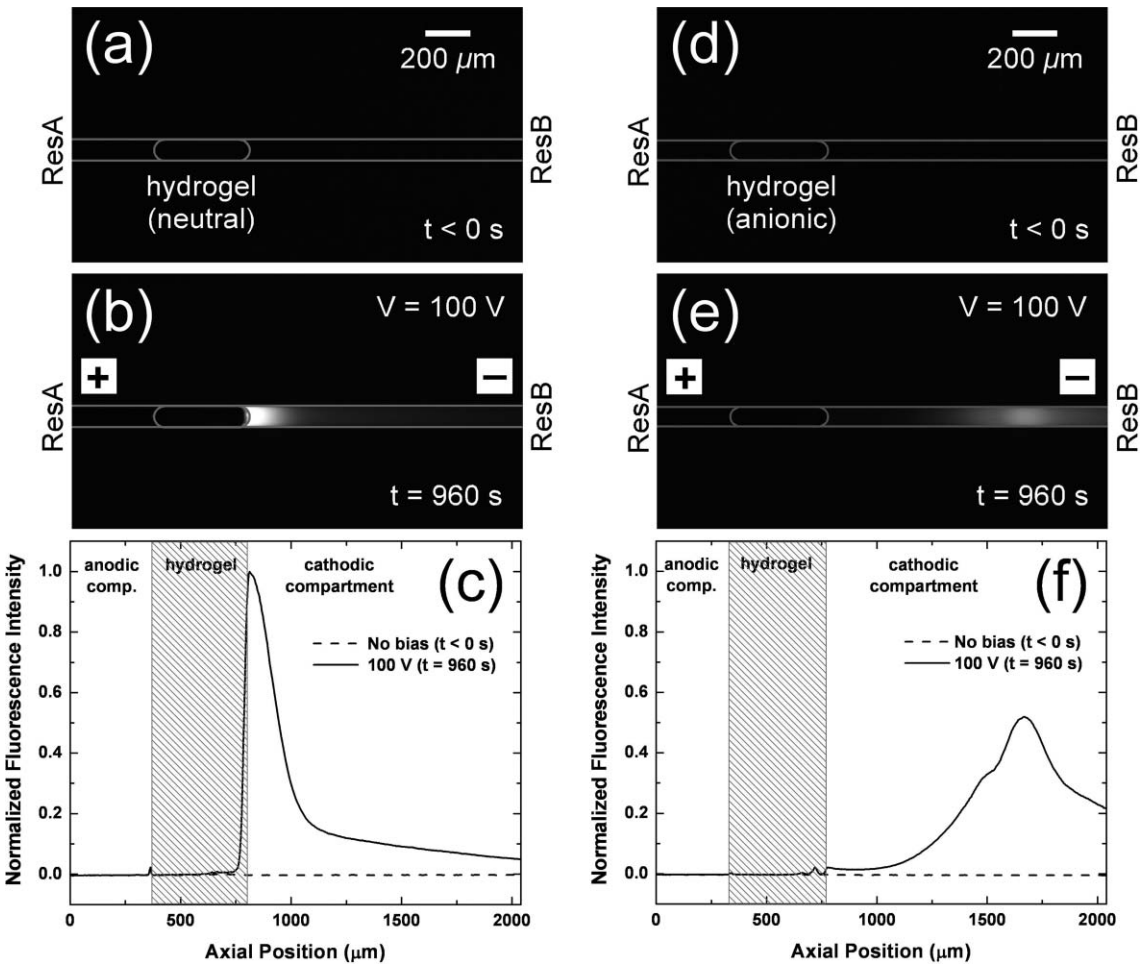

Fig. 2 Fluorescence micrographs for BSA obtained in the microfluidic device (layout shown in Fig. 1a) with a neutral (a–c) or anionic (d–f) hydrogel microplug before (a, d), and after (b, e) applying a forward bias of 100 V for 960 s. (c) and (f) represent the corresponding fluorescence intensity profiles obtained parallel to the channel during the forward bias experiment. The covered axial position ($x = 0$–2000 μm) corresponds to the dimension of the microscopic focus, while the distance between the electrodes is *ca.* 8.25 mm (*cf*. Fig. 1a).

Fig. 2c shows fluorescence intensity profiles corresponding to the micrographs of Fig. 2a and 2b. No significant fluorescence intensity is observed in the hydrogel for BSA during application of the forward bias, except at the very edge of the microplug. This small amount of concentration is an artifact of how the interface between hydrogel and solution is defined: that is, the actual interface is not planar and hence larger than the resolution of the camera used to obtain images. Clearly, however, BSA is size-excluded from the hydrogel, and it therefore concentrates at/close to the cathodic hydrogel plug–microchannel solution interface. The concentration enrichment was ~ 400-fold at an applied bias of 100 V (*ca.* 12 kV m^{-1}) for 960 s.

Anionic hydrogel microplug as a physical and ion-permselective barrier

The presence of negative charges on the hydrogel plug results in a different behavior compared to the neutral hydrogel. Fig. 2d and 2e are fluorescence micrographs obtained for BSA in a channel containing the negative hydrogel, but under the same conditions used for the neutral hydrogel. As with the neutral hydrogel, BSA is transported electrophoretically towards the plug under the influence of a 100 V bias. However, BSA fails to reach the cathodic hydrogel plug–microchannel solution interface and instead concentrates in the bulk solution of the cathodic compartment (Fig. 2e). Fig. 2f shows corresponding fluorescence intensity profiles obtained along the microchannel before and after application of the forward bias. The concentration enrichment factor, which corresponds to the peak intensity, in this case was ~130 only.

Concentration enrichment factors for BSA obtained during the forward bias are compared for neutral and anionic hydrogel in Fig. 3. In both cases, there is a sudden rise in the enrichment factors within 120 s after the application of the electrical field. These enrichment factors for BSA begin to level off for $t > 120$ s. The neutral hydrogel demonstrates an ~400-fold concentration enrichment at an electrical bias of 100 V. In order to achieve a similar enrichment factor with the anionic hydrogel a much higher electrical bias (300 V) is required, whereas a bias of 100 V results in enrichment factors of up to only ~130.

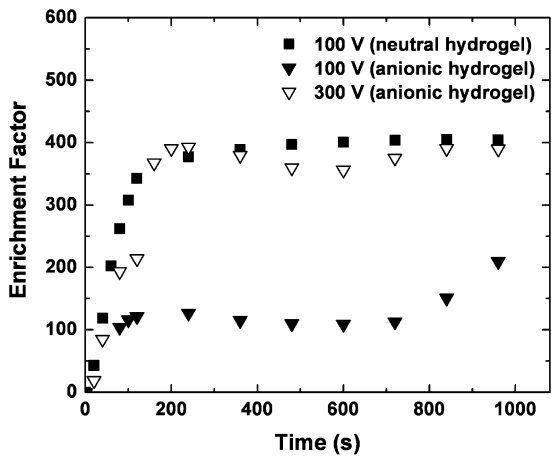

Fig. 3 Enrichment factors obtained in the cathodic microchannel compartment for BSA as a function of time employing a neutral hydrogel microplug at 100 V bias and an anionic hydrogel microplug at 100 V and 300 V bias.

Numerical simulations

For analyzing the interplay of fixed charge on the hydrogel backbone, the spatiotemporal distribution of electrolyte ions and local electrical field, as well as concentration enrichment efficiency, we conducted a set of numerical simulations for membranes with the following values of negative fixed-charge of uniform volume density (*cf*. Table 1): $c_{fix} = 0$ (neutral membrane), $c_{fix} = 0.1c_{res}$ (weakly charged membrane), and $c_{fix} = c_{res}$ (highly charged membrane), where c_{res} is the bulk (reservoir) concentration of the background electrolyte. At electrochemical equilibrium the Donnan potential (ψ_D) of a membrane relative to the bulk electrolyte solution external to the membrane is expressed as

$$\psi_D = -\frac{RT}{zF}\,\mathrm{arc\,sinh}\left(\frac{c_{fix}}{2zc_{res}}\right), \quad (3)$$

where z is the valency of the ions of the (symmetrical) background electrolyte. For $T = 297$ K and $z = 1$, eqn (3) gives $\psi_D = -1.279$ mV and -12.33 mV for $c_{fix} = 0.1c_{res}$ and $c_{fix} = c_{res}$, respectively. In our simulations, the corresponding values were -1.280 mV and -12.36 mV. Thus, the relative differences between theoretical and simulated values of the Donnan potential did not exceed 0.33%. These values of ψ_D demonstrate the substantial difference between weakly and highly charged membranes concerning their ion-permselectivity. Fig. 4 and 5 show that this difference is also manifested in the intensity of CP which develops after the application of an external electrical field of $E_{ext} = 11.1$ kV m^{-1}.

A nanoporous hydrogel with fixed negative charges acts as a cation-selective membrane. It enriches cations (counterions), but excludes anions (co-ions) from its nanopore space (Donnan exclusion).[26–29] After the application of an electrical field CP develops in the bulk electrolyte solutions next to an anionic hydrogel plug or membrane (Fig. 4). It is the consequence of coupled mass and charge transport through the ion-permselective interfaces.[26,27] On the side of a cation-selective membrane where counterions enter the membrane in the direction of the applied field (anodic interface), the local interplay of diffusion and electromigration results in a diffusion boundary layer (DBL) with reduced ion concentrations relative to the bulk solution (Fig. 4: $x = 0$–800 μm; *cf*. Fig. 1b). This anodic DBL comprises a depleted CP zone: as the field is switched on, co-ions move away from the anodic interface (towards the anode), but their local withdrawal cannot be compensated by the few co-ions which actually remain inside the hydrogel due to its cation-selectivity (co-ion exclusion). The co-ion concentration decreases locally in the solution adjacent to the anodic interface and so does the counterion concentration to maintain local electroneutrality. At the cathodic interface where counterions leave the membrane, the electrolyte concentration correspondingly increases. This cathodic DBL results in an enriched CP zone (Fig. 4a: $x =$ 1200–2000 μm; *cf*. Fig. 1b).

The extended CP zones affect local conductivity and result in a redistribution of the local electrical field within the system: the local electrical field in the cathodic compartment is reduced

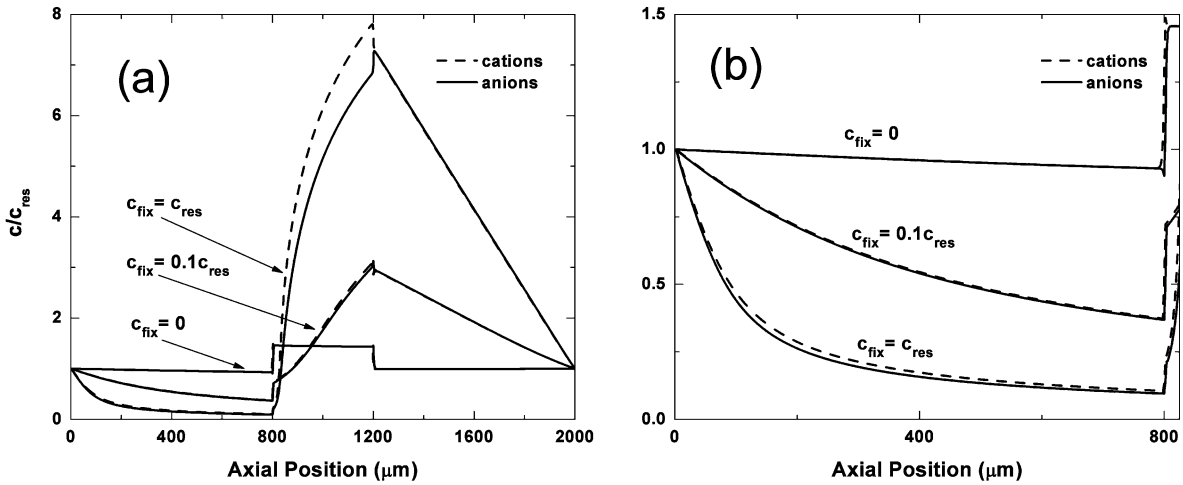

Fig. 4 Steady-state concentration distributions for cations and anions of the background electrolyte obtained after application of an electrical field (E_{ext}) of 11.1 kV m^{-1} along the microchannel containing a neutral ($c_{fix} = 0$), a weakly charged ($c_{fix} = 0.1c_{res}$), or a highly charged membrane ($c_{fix} = c_{res}$). (a) Whole microchannel ($x = 0$–2000 μm); (b) anodic compartment enlarged. The membranes occupy the region $x = 800$–1200 μm. In contrast to Fig. 2 the covered axial position ($x = 0$–2000 μm) here corresponds directly to the distance between the electrodes (*cf*. Fig. 1b).

much below that in case of the neutral membrane (Fig. 5). Thus, the electrophoretic driving force in the cathodic compartment is considerably weaker with the anionic hydrogel, and in turn is responsible for a smaller concentration enrichment of analytes like BSA as shown experimentally in Fig. 2 and 3. In addition, the presence of fixed charges on the hydrogel leads to an electroosmotic flow inside the hydrogel nanopores, in conjunction with electroosmotic flow generated in the microchannels,[22] which is reflected in the experiments by a displacement of the analyte zone away from the cathodic hydrogel plug–microchannel solution interface (Fig. 2f and part (b) of Scheme 1).[37]

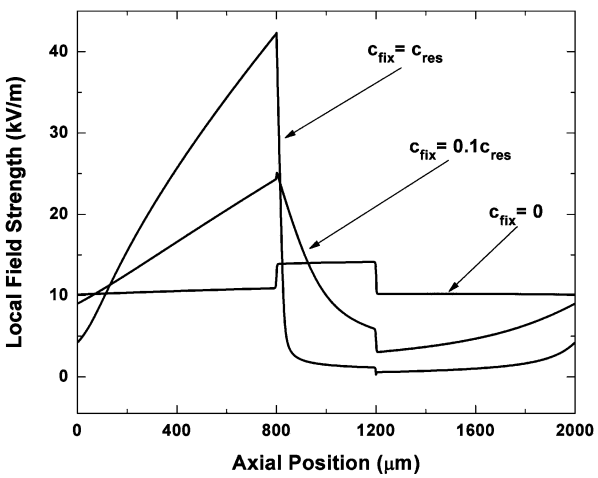

Fig. 5 Steady-state distribution of the local electrical field strength for an applied field of $E_{ext} = 11.1$ kV m^{-1}. The membranes occupy the region $x = 800$–1200 μm.

The depleted CP zone—the region of the lowest electrolyte concentration and highest electrical resistance—results in a strong local potential drop (electrical field) in the anodic microchannel compartment (Fig. 5: $x = 0$–800 μm), while the opposite is observed with the enriched CP zone in the cathodic compartment ($x = 1200$–2000 μm). With respect to the weakly charged membrane ($c_{fix} = 0.1c_{res}$), the results for the membrane with $c_{fix} = c_{res}$ demonstrate a much more intense CP (Fig. 4). In particular, the species distributions in the anodic depleted CP zone for the highly charged membrane provide evidence for the two spatial domains of the depleted CP zone under nonequilibrium conditions:[43–48] (i) the electroneutral part of the quiescent DBL (towards the buffer reservoir) with a nearly linear variation of the species concentrations, and (ii) a space charge region (in the bulk liquid between the anodic membrane–solution interface and the electroneutral part of the depleted CP zone) which is the mobile part of an electric field-induced electrical double layer. By contrast, in the cathodic enriched CP zone we observe a linear variation of species concentrations (Fig. 4a: $x = 1200$–2000 μm) at any field strength.

An enlarged view of the anodic depleted CP zone ($x = 0$–800 μm) is shown in Fig. 4b. The concentration of counterions exceeds that of the co-ions over a substantial region under nonequilibrium conditions (highly charged membrane; $c_{fix} = c_{res}$). The mobile positive space charge in the anodic depleted CP zone is compensated by unscreened fixed negative surface charge of the membrane, namely inside the membrane at/very close to the anodic membrane–solution interface. This electric field-induced electrical double layer forms the basis for a nonlinear electrokinetics.[26] Consequences of the mobile space charge region, however, cannot be studied further within the one-dimensional model, because the investigation of the coupling between electrokinetics and hydrodynamics requires at least a two-dimensional model.

For the present analysis of concentration enrichment efficiencies with an uncharged, a weakly and a highly charged membrane the implication of the different intensities of CP is, however, very clear: the stronger the resulting CP at a given field strength (due to the increasing ion-permselectivity of a membrane; Fig. 4), the smaller the local field strength at the cathodic membrane–solution interface of the membrane (Fig. 5) responsible for steady-state concentration enrichment. This is caused by the fact that electrical potential drop in the

anodic depleted CP zone increases with the membranes ion-permselectivity. For example, at an applied field strength of 11.1 kV m^{-1} we find local field strengths of up to 40 kV m^{-1} in the anodic depleted CP zone of the system with the highly charged membrane ($c_{fix} = c_{res}$), while electrical field strength next to the cathodic membrane–solution interface drops below 1 kV m^{-1} (Fig. 5). For the sake of completeness we point out that (yet small) differences in electrical field distribution in the anodic and cathodic microchannel compartments also develop with the neutral membrane (Fig. 5, $c_{fix} = 0$). Caused by the concentration enrichment of charged tracer and ion redistribution the field strength in the cathodic compartment (x = 1200–2000 μm) is slightly smaller than in the anodic compartment (x = 0–800 μm), while inside the membrane (x = 800–1200 μm) the field strength is higher than in both adjoining microchannel compartments due to the required conservation of electrical flux in the interconnected system and the fact that the diffusion coefficient of the background ions inside the membrane is reduced with respect to the bulk microchannel solutions.

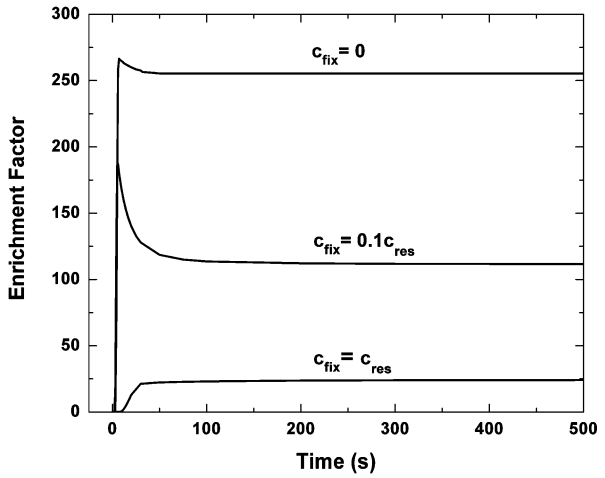

Fig. 6 Transient behavior of enrichment factors for a negatively charged, size-excluded analyte at an applied electrical field of E_{ext} = 11.1 kV m^{-1} in the microchannel (*cf*. Fig. 1b) containing a neutral ($c_{fix} = 0$), a weakly charged ($c_{fix} = 0.1c_{res}$), or a highly charged membrane ($c_{fix} = c_{res}$).

The above conclusion about the effect of the volume density of fixed charge of a membrane on its performance in electrokinetic concentration enrichment is confirmed by Fig. 6, where we present the transient behavior of the enrichment factors obtained for the neutral, the weakly and the highly charged membranes. In our simulations the neutral membrane yielded steady-state enrichment factors more than 10 times higher than for the highly charged membrane. The overshoot in the enrichment factor with the weakly charged membrane ($c_{fix} = 0.1c_{res}$) is much stronger than for the neutral one (Fig. 6). It can be explained by the fact that CP is not fully developed when the analyte molecules begin to reach the cathodic membrane–solution interface. The analyte arrives at the membrane during the formation of CP and, for the cathodic membrane–solution interface, this means that the local electrolyte concentration increases, while the local electrical field strength decreases. Since the amount of analyte introduced into the cathodic microchannel compartment is assumed to be fixed, it results in a redistribution of the analyte concentration in order to keep a local balance between diffusive and electrophoretic fluxes. This is confirmed, in particular, by the transient behaviour of the local electrical field at the cathodic membrane–solution interface;[37] its decrease during the formation of CP leads to a reduction of electromigration flux towards the membrane. In turn, this results in a drop of the amplitude of the analyte enrichment zone because back-diffusion flux is not affected by the local field strength. At the same time, for the highly charged membrane ($c_{fix} = c_{res}$) the initial overshoot in the enrichment factor was not observed. It can be explained by the stronger CP, resulting in a lower electromigration velocity of the analyte because of the reduced field strength in the cathodic microchannel compartment. As a consequence, analyte molecules reach the cathodic membrane–solution interface after the CP is fully developed.

Fig. 7a plots the steady-state enrichment factors as a function of the externally applied field strength (E_{ext}). The nonlinear behaviour can be explained by the constant amount of analyte which is used in the simulations for enrichment at a membrane. Higher peak intensities (at higher field strengths) stimulate a stronger diffusive broadening which results in a smaller increase of the enrichment factor than based on a linear scaling with

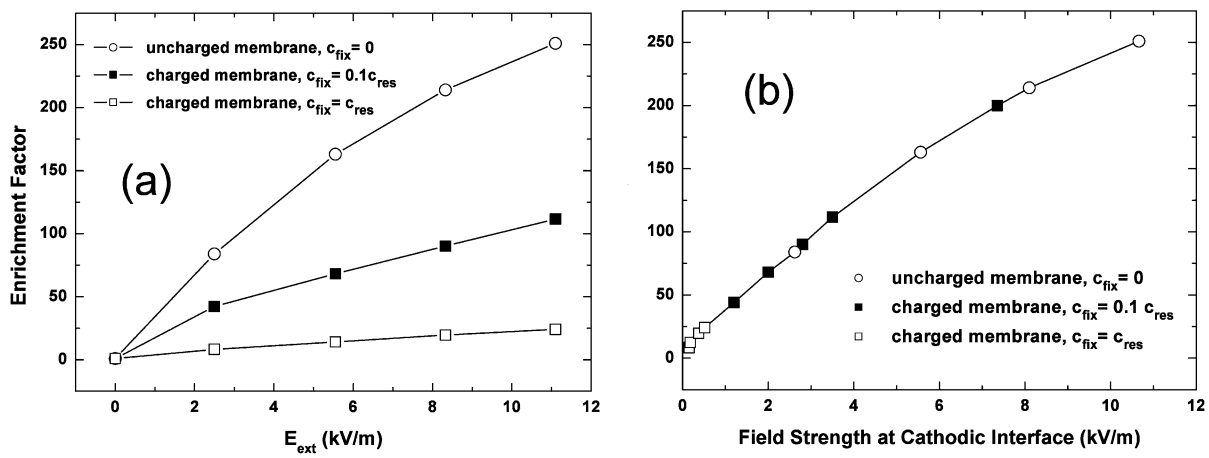

Fig. 7 Steady-state enrichment factors as a function of (a) the applied electrical field strength and (b) the local electrical field strength at the cathodic membrane–bulk solution interface (data for the neutral, weakly charged and highly charged membranes plotted together).

the applied field strength. The results of the simulations in Fig. 6 and 7a are in agreement with the experimental results presented in Fig. 3. Both results demonstrate the need for applying stronger electrical fields to a charged hydrogel or membrane to realize the same enrichment factor (*i.e.*, the same local field strength at the cathodic membrane–solution interface) as for the neutral hydrogel or membrane. In particular, we note the good agreement between the experimental data for the anionic hydrogel at an applied bias of 100 V (*ca.* 12 kV m^{-1}, Fig. 3) and the simulated data for the weakly ion-permselective membrane at $E_{ext} = 11.1$ kV m^{-1} (Fig. 7a, last solid square). Similar enrichment factors of 110–130 are observed in both cases. In addition, applied electrical field strengths must be increased by about three times in order to achieve the enrichment factors realized with the corresponding neutral hydrogel or membrane.

If we plot the enrichment factors against local field strength at the cathodic membrane–solution interface, all events result in one conclusive picture (Fig. 7b): enrichment factors for the different membranes (neutral, weakly charged, highly charged) collapse onto a single curve. This demonstrates that the enrichment factor scales with the locally effective field strength which, in turn, is governed by the actual intensity of CP in the system, basically, by how much of the electrical potential drop occurs in the anodic depleted CP zone (*cf*. Fig. 5). In addition to the data of Fig. 7a we have included in Fig. 7b the result of another simulation with the weakly charged membrane ($c_{fix} = 0.1c_{res}$) at a still higher field strength ($E_{ext} = 22.2$ kV m^{-1}) than in Fig. 7a in order to corroborate the unique trend evidenced by Fig. 7b. As seen, the resulting enrichment factor (~ 200) excellently fits into the general curve if plotted against the locally effective field strength (*ca.* 7.4 kV m^{-1}).

Summary and conclusions

We have evaluated the relative performance of neutral and anionic hydrogel microplugs in concentrating charged analytes in a microfluidic device which contains a straight microfluidic channel with the respective nanoporous plug fixed at its center (Fig. 1). Results are described in terms of the concentration enrichment for analytes which are size-excluded from any of the hydrogels (Scheme 1). The neutral hydrogel is used as a simple size-exclusion filter with respect to the electrophoretic transport of charged analytes, resulting in concentration enrichment at the hydrogel boundary (Fig. 2). A negatively charged nanoporous hydrogel, in addition, is ion-permselective. The application of an electrical field across the anionic hydrogel leads to CP due to coupled mass and charge transport of the small enough electrolyte ions through the ion-permselective hydrogel plug–bulk solution interfaces (Fig. 4). The concentration enrichment of size-excluded analyte molecules with the anionic hydrogel is less efficient compared to the neutral hydrogel owing to the CP-based redistribution of the local electrical field (Fig. 5 and 6).

The described experiments and simulations explain the functionality of nanoporous membranes differing in their ion-permselectivity for concentration enrichment on multifunctional lab-on-a-chip platforms useful for many analytes. CP in the operational mode investigated in this work is an undesired side effect with the anionic hydrogels: it reduces the local electrical field strength driving concentration enrichment of negatively charged analytes (which are introduced from the cathodic reservoir) at/close to the cathodic hydrogel plug–microchannel solution interface (Fig. 5). In principle, this effect can be compensated by applying (much) higher field strengths across a (highly) charged compared with a neutral membrane (Fig. 7). However, the corresponding field strengths may limit device performance and scalability due to Joule heating and complex (electro)hydrodynamic phenomena originating in the anodic depleted CP zone under nonequilibrium conditions.

Finally, it should be mentioned that the analysis presented here is also relevant to devices in which a discrete nanochannel, instead of a nanoporous membrane (in which many nanopores are interconnected in a usually nontrivial fashion), is used to interconnect the two microchannel compartments.[26,49–53] Then, with a charged and ion-permselective nanochannel interconnect, as in this work with the charged membranes, CP is an intimate companion, either as a prerequisite or as an undesired side effect (or both) with respect to device functionality and performance.

Acknowledgements

RMC and RD acknowledge the U. S. Department of Energy, Office of Basic Energy Sciences (Contract No. DE-FG02-01ER15247) and the U. S. Army Research Office/Defense Threat Reduction Agency (Grant No. W911NF-07-1-0330) for supporting this work. UT and DH acknowledge the Deutsche Forschungsgemeinschaft DFG (Bonn, Germany) for supporting this work under grants TA 268/2 and HL 56/1.

References

1 D. S. Peterson, *Lab Chip*, 2005, **5**, 132–139.
2 J. de Jong, R. G. H. Lammertink and M. Wessling, *Lab Chip*, 2006, **6**, 1125–1139.
3 P. A. Walker, III, M. D. Morris, M. A. Burns and B. N. Johnson, *Anal. Chem.*, 1998, **70**, 3766–3769.
4 P. G. Righetti and A. Bossi, *Anal. Chim. Acta*, 1998, **372**, 1–19.
5 J. P. Quirino and S. Terabe, *Anal. Chem.*, 1999, **71**, 1638–1644.
6 J. Khandurina, S. C. Jacobson, L. C. Waters, R. S. Foote and J. M. Ramsey, *Anal. Chem.*, 1999, **71**, 1815–1819.
7 J. Han and H. G. Craighead, *Science*, 2000, **288**, 1026–1029.
8 R. D. Oleschuk, L. L. Shultz-Lockyear, Y. Ning and D. J. Harrison, *Anal. Chem.*, 2000, **72**, 585–590.
9 J. Lichtenberg, E. Verpoorte and N. F. de Rooij, *Electrophoresis*, 2001, **22**, 258–271.
10 Y. Sera, N. Matsubara, K. Otsuka and S. Terabe, *Electrophoresis*, 2001, **22**, 3509–3513.
11 P. C. Wang, D. L. DeVoe and C. S. Lee, *Electrophoresis*, 2001, **22**, 3857–3867.
12 C. Yu, M. H. Davey, F. Svec and J. M. J. Frechet, *Anal. Chem.*, 2001, **73**, 5088–5096.
13 G. M. Walker and D. J. Beebe, *Lab Chip*, 2002, **2**, 57–61.
14 D. Ross and L. E. Locascio, *Anal. Chem.*, 2002, **74**, 2556–2564.
15 J. Lichtenberg, N. F. de Rooij and E. Verpoorte, *Talanta*, 2002, **56**, 233–266.
16 B. Jung, R. Bharadwaj and J. G. Santiago, *Electrophoresis*, 2003, **24**, 3476–3483.
17 R.-L. Chien, *Electrophoresis*, 2003, **24**, 486–497.
18 B. S. Broyles, S. C. Jacobson and J. M. Ramsey, *Anal. Chem.*, 2003, **75**, 2761–2767.
19 S. Song, A. K. Singh and B. J. Kirby, *Anal. Chem.*, 2004, **76**, 4589–4592.

20 D. Erickson and D. Li, *Anal. Chim. Acta*, 2004, **507**, 11–26.
21 R. S. Foote, J. Khandurina, S. C. Jacobson and J. M. Ramsey, *Anal. Chem.*, 2005, **77**, 57–63.
22 R. Dhopeshwarkar, L. Sun and R. M. Crooks, *Lab Chip*, 2005, **5**, 1148–1154.
23 S. Song and A. K. Singh, *Anal. Bioanal. Chem.*, 2006, **384**, 41–43.
24 R. T. Kelly, Y. Li and A. T. Woolley, *Anal. Chem.*, 2006, **78**, 2565–2570.
25 A. V. Hatch, A. E. Herr, D. J. Throckmorton, J. S. Brennan and A. K. Singh, *Anal. Chem.*, 2006, **78**, 4976–4984.
26 A. Höltzel and U. Tallarek, *J. Sep. Sci.*, 2007, **30**, 1398–1419.
27 *Surface Chemistry and Electrochemistry of Membranes*, ed. T. S. Sørensen, Marcel Dekker, New York, 1999.
28 F. Helfferich, *Ion Exchange*, McGraw-Hill, New York, 1962.
29 F. G. Donnan, *J. Membr. Sci.*, 1995, **100**, 45–55.
30 M. Nishizawa, V. P. Menon and C. R. Martin, *Science*, 1995, **268**, 700–702.
31 C. R. Martin, M. Nishizawa, J. Jirage and M. Kang, *J. Phys. Chem. B*, 2001, **105**, 1925–1934.
32 S. B. Lee and C. R. Martin, *Anal. Chem.*, 2001, **73**, 768–775.
33 K.-Y. Chun and P. Stroeve, *Langmuir*, 2002, **18**, 4653–4658.
34 P. Ramirez, S. Mafé, A. Alcaraz and J. Cervera, *J. Phys. Chem. B*, 2003, **107**, 13178–13187.
35 J.-R. Ku and P. Stroeve, *Langmuir*, 2004, **20**, 2030–2032.
36 K.-Y. Chun, S. Mafé, P. Ramirez and P. Stroeve, *Chem. Phys. Lett.*, 2006, **418**, 561–564.
37 R. Dhopeshwarkar, R. M. Crooks, D. Hlushkou and U. Tallarek, *Anal. Chem.*, 2008, **80**, 1039–1048.
38 J. C. McDonald, D. C. Duffy, J. R. Anderson, D. T. Chiu, W. Hongkai, O. J. A. Schueller and G. M. Whitesides, *Electrophoresis*, 2000, **21**, 27–40.
39 P. B. Warren,, *Int. J. Mod. Phys. C*, 1997, **8**, 889–898.
40 F. Capuani, I. Pagonabarraga and D. Frenkel, *J. Chem. Phys.*, 2004, **121**, 973–986.
41 T. Peters, Jr., *Adv. Protein Chem.*, 1985, **37**, 161–245.
42 T. Canal and N. A. Peppas, *J. Biomed. Mater. Res.*, 1989, **23**, 1183–1193.
43 Y. Ben and H.-C. Chang, *J. Fluid Mech.*, 2002, **461**, 229–238.
44 V. I. Zabolotskii, J. A. Manzanares, S. Mafé, V. V. Nikonenko and K. A. Lebedev, *Russ. J. Electrochem.*, 2002, **38**, 819–827.
45 I. Rubinshtein, B. Zaltzman, J. Pretz and C. Linder, *Russ. J. Electrochem.*, 2002, **38**, 853–863.
46 V. M. Volgin and A. D. Davydov, *J. Membr. Sci.*, 2005, **259**, 110–121.
47 E. Quenneville and M. D. Buschmann, *J. Membr. Sci.*, 2005, **265**, 60–73.
48 B. Zaltzman and I. Rubinstein, *J. Fluid Mech.*, 2007, **579**, 173–226.
49 Q. Pu, J. Yun, H. Temkin and S. Liu, *Nano Lett.*, 2004, **4**, 1099–1103.
50 Y.-C. Wang, A. L. Stevens and J. Han, *Anal. Chem.*, 2005, **77**, 4293–4299.
51 S. M. Kim, M. A. Burns and E. F. Hasselbrink, *Anal. Chem.*, 2006, **78**, 4779–4785.
52 S. J. Kim, Y.-C. Wang, J. H. Lee, H. Jang and J. Han, *Phys. Rev. Lett.*, 2007, **99**, 044501.
53 T. A. Zangle, A. Mani and J. G. Santiago, *Proceedings of the Eleventh International Conference on Miniaturized Systems for Chemistry and Life Sciences*, Paris, 2007, pp. 1204–1206.

